Modeling Mixed Poisson-Gaussian Noise in Statistical Image Reconstruction for X-Ray CT

Qiaoqiao Ding, Yong Long, Xiaoqun Zhang and Jeffrey A. Fessler

***Abstract*—Statistical image reconstruction (SIR) methods for X-ray CT improve the ability to produce high-quality and accurate images, while greatly reducing patient exposure to radiation. The challenge with further dose reduction to an ultra-low level by lowering the X-ray tube current is photon starvation and electronic noise starts to dominate. This introduces negative or zero values into the raw data and consequently causes artifacts in the reconstructed CT images with current SIR methods based on log data. At ultra-low photon counts, the CT detector signal deviates significantly from Poisson or shifted Poisson statistics for the pre-log data and from Gaussian statistics for post-log data. This paper proposes a novel SIR method called MPG (mixed Poisson-Gaussian). It models the raw noisy measurements using a mixed Poisson-Gaussian distribution that accounts for the electronic noise. The MPG method is able to directly use the negative and zero values in the raw data without any pre-processing. We adopt the reweighted least square method to develop a tractable likelihood function that can be easily incorporated into SIR reconstruction framework. To minimize the MPG cost function containing the likelihood function and an edge-preserving regularization term, we use an Alternating Direction Method of Multipliers (ADMM) that divides the o-riginal optimization problem into several sub-problems that are easier to solve. Our results on 3D simulated cone-beam data set indicate that the proposed MPG method reduces noise in the reconstructed images comparing with the conventional FBP and statistical penalized weighted least-square (PWLS) method for ultra-low dose CT (ULDCT) imaging.**

I. Introduction

X-Ray Computed Tomography (CT) provides high-resolution images of anatomical structures for diagnosis and management of human diseases and disorders. For example, CT has had a tremendous impact on cancer. Studies have suggested that current CT usage may be responsible for 1.5%-2% of all cancers in the U.S. [1]. Significantly lowering radiation dosages from CT has become a growing concern both in the public and professional societies. Ultra-low dose CT (ULDCT) scans that still provide suitable image quality could shift CT scans further to the benefit side and open up numerous entirely new clinical applications.

CT image reconstruction method improvements that could realistically and significantly reduce patient radiation exposure while maintaining high image quality is an important area of research to achieve low dose CT imaging. Statistical image reconstruction (SIR) methods [2] improve the ability to produce high-quality and accurate images, while greatly reducing patient exposure to radiation. The challenge with further dose reduction to an ultra-low level by reducing the number of projection views is the aliasing artifacts due to under-sampled sinograms when the number of views is too small [3]. An alternative approach is to lower the X-ray tube current, but this causes photon starvation and electronic noise starts to denominate [4]. This approach introduces negative or zero values into the raw data and consequently causes artifacts in the reconstructed CT images with current data processing methods [5] based on log sinogram data.

The measurement statistical models in most SIR methods assume standard or shifted Poisson statistics for the pre-log data or Gaussian distributions for the post-log data. At ultra-low photon counts, the CT measurements deviate significantly from Poisson or Gaussian statistics. For ULDCT imaging the logarithm simply cannot be used because the raw data have negative or zero values due to the electronic noise in the data acquisition systems (DAS). In [6], the authors substituted the non-positive measurements with a small positive value. Poisson distribution models the number of events which should be non-negative. The shifted Poisson model adds a positive value associated with the variance of electronic noise to the raw data, but the shifted raw data may still be negative or zero for ULDCT imaging. Compound Poisson (CP) distribution [7], [8] that accounts for the polyenergetic X-rays and Poisson light statistics in the scintillator of energy-integrating detector has the potential to accurately model the measurement statistics in ULDCT imaging. However, CP model has a complicated likelihood that impedes direct use in SIR methods and electronic readout noise leads to a distribution that is even more complicated than a CP model.

This paper proposes a new SIR method with a data-fit term associated with the mixed Poisson-Gaussian (MPG) distribution model for CT measurements [9], [10] and the edge-preserving hyperbola regularization. The proposed MPG method is able to directly process negative or zero valued raw data that contain (some, albeit limited) information about the scanned object. We solve the MPG optimation problem using Alternating Direction Method of Multipliers (ADMM, also known as split Bregman method [11]) and its unconstrained subproblems using Conjugate Gradient (CG), Broyden-Fletcher-Goldfarb-Shanno (BFGS).

This paper is organized as follows. Section II mathematically formulates the MPG method for X-ray CT reconstruction as a Penalized-Likelihood (PL) cost function and solves it

Q. Ding (e-mail: dingqiaoqiao@sjtu.edu.cn) and X. Zhang (e-mail: xqzhang@sjtu.edu.cn) are with School of Mathematical Sciences and Institute of Natural Sciences, Shanghai Jiao Tong University. 800, Dongchuan Road, Shanghai, China, 200240

Y. Long (e-mail: yong.long@sjtu.edu.cn) is with the University of Michigan- Shanghai Jiao Tong University Joint Institute, Shanghai Jiao Tong University, 800 Dongchuan Road, Shanghai, China, 200240

J. A. Fessler (e-mail: fessler@umich.edu) is with the Department of Electrical Engineering and Computer Science, University of Michigan, Ann Arbor, MI 48109.

using ADMM. Section III presents numerical experiments and results. Finally, we draw our conclusions in Section IV.

II. Methods

A. Measurement Model

Let y_i denote the number of X-ray photons incident on detector for the ith ray where $i = 1, \cdots, N_d$, and N_d is the number of rays. For a monoenergetic source, we model the number of X-ray photons as :

$$\bar{y}_i = \bar{y}_i(\boldsymbol{x}) \triangleq I_i \exp(-[\boldsymbol{A}\boldsymbol{x}]_i) + r_i \tag{1}$$

where $\boldsymbol{x}$ denotes the attenuation map, and its jth element x_j is the average linear attenuation coefficient in the jth voxel for $j = 1, \cdots, N_p$, where N_p denotes the number of voxels. $\boldsymbol{A}$ is the $N_d \times N_p$ system matrix with entries a_{ij}, and $[\boldsymbol{A}\boldsymbol{x}]_i = \sum_{j=1}^{N_p} a_{ij} x_j$ denotes the line integral of the attenuation map $\boldsymbol{x}$ along the ith X-ray. We treat each I_i and r_i as known nonnegative quantities, where r_i is ensemble mean of background signals such as Compton, scatter and dark current, and I_i is the incident X-ray intensity incorporating X-ray source illumination and the detector gain. Although the measurement model in (1) ignores beam-hardening effects [12], [13], polyenergetic measurement models that account for the source spectrum and energy-dependent attenuation will be employed in our future work.

For the case of normal clinical exposures, the X-ray CT measurements z_i are often modeled as the sum of a Poisson distribution representing photon-counting statistics (1) and an independent Gaussian distribution representing additive electronic noise:

$$z_i = k y_i + y_e \tag{2}$$

where $y_i \sim \text{Poisson}(\bar{y}_i(\boldsymbol{x}))$ and $y_e \sim \text{N}(0, \sigma^2)$, k is a scalar factor modeling the conversion gain from X-ray photons to electrons and σ denotes the standard deviation of electronic noise.

B. Penalized Weighted Least Square for Poisson-Gaussian Mixed Noise

We adopt the reweighted least square method [10] to develop a tractable likelihood function for the mixed Poisson-Gaussian measurement statistical model. Given $\bar{y}_i$, Assuming y_i and y_e are independent, we have

$$\text{E}[z_i] = k\text{E}[y_i] = k\bar{y}_i$$

and

$$\text{Var}[z_i] = k^2\text{Var}[y_i] + \text{Var}[y_e] = k^2\bar{y}_i + \sigma^2$$

We approximate z_i with normal distribution, i.e., $z_i \sim N(k\bar{y}_i, k^2\bar{y}_i + \sigma^2)$, i.e., the Probability Density Function (PDF) of z_i is

$$P(z_i; \boldsymbol{x}) = \frac{1}{\sqrt{2\pi(k^2\bar{y}_i(\boldsymbol{x}) + \sigma^2)}} e^{-\frac{(z_i - k\bar{y}_i(\boldsymbol{x}))^2}{2(k^2\bar{y}_i(\boldsymbol{x}) + \sigma^2)}} \tag{3}$$

The corresponding approximate negative log-likelihood for independent measurements z_i has the form

$$\bar{L}(\boldsymbol{x}) = -\sum_{i=1}^{N_d} \log(P(z_i; \boldsymbol{x})) \equiv \frac{1}{2}\|\boldsymbol{z} - k\bar{\boldsymbol{y}}(\boldsymbol{x})\|^2_{\boldsymbol{W}(\boldsymbol{x})} + \frac{1}{2}\langle \log(k^2\bar{\boldsymbol{y}}(\boldsymbol{x}) + \boldsymbol{\sigma}^2), \boldsymbol{1}\rangle, \tag{4}$$

where $\equiv$ means "equal to within irrelevant constants independent of $\boldsymbol{x}$", the diagonal weight matrix $\boldsymbol{W}(\boldsymbol{x})$ is

$$\boldsymbol{W}(\boldsymbol{x}) = \text{diag}\left\{\frac{1}{k^2\bar{y}_i(\boldsymbol{x}) + \sigma^2}\right\}, \tag{5}$$

$\boldsymbol{z} \in \mathbb{R}^{N_d}$ and $\bar{\boldsymbol{y}}(\boldsymbol{x}) \in \mathbb{R}^{N_d}$ have elements of z_i and $\bar{y}_i(\boldsymbol{x})$ respectively, $\boldsymbol{\sigma}^2 \in \mathbb{R}^{N_d}$ and $\boldsymbol{1} \in \mathbb{R}^{N_d}$have every element equal to σ^2 and 1 respectively, and $\langle \cdot, \cdot \rangle$ is inner product. $\log(\cdot)$ is pointwise operation. We estimate the attenuation map $\boldsymbol{x}$ from the noisy measurements $\boldsymbol{z}$ by minimizing a Penalized-Likelihood (PL) cost function as follows:

$$\hat{\boldsymbol{x}} = \arg\min_{\boldsymbol{x}} \Psi(\boldsymbol{x}) \tag{6}$$

$$\Psi(\boldsymbol{x}) \triangleq \bar{L}(\boldsymbol{x}) + R(\boldsymbol{x}). \tag{7}$$

The regularization term $R(\boldsymbol{x})$ is

$$R(\boldsymbol{x}) = \lambda \sum_{i=1}^{N_r} \beta_r \psi_r([\boldsymbol{C}\boldsymbol{x}]_r), \tag{8}$$

where the regularization parameter λ controls the noise and resolution tradeoff, β_r is the spatial weighting, $\psi_r(\cdot)$ is a potential function, $\boldsymbol{C} \triangleq \{C_{rj}\} \in \mathbb{R}^{N_r \times N_p}$is a sparsifying matrix finite-differencing matrix and $[\boldsymbol{C}\boldsymbol{x}]_r = \sum_{j=1}^{N_p} C_{rj} x_j$. We focus on edge-preserving hyperbola regularization, i.e, $\psi_r(t) = \delta^2(\sqrt{(\frac{t}{\delta})^2 + 1} - 1)$. The regularization term $R(x)$ can be written as $R(x) = \lambda\delta^2(\sqrt{(\frac{\boldsymbol{C}\boldsymbol{x}}{\delta})^2 + 1} - 1)$.

C. Optimization Method

1) Equivalent Optimization Model: Because (6) is hard to solve directly, we introduce auxiliary variables $\boldsymbol{u} \in \mathbb{R}^{N_d}, \boldsymbol{v} \in \mathbb{R}^{N_r}$. Then, we rewrite our problem as the following equivalent constrained problem:

$$\begin{aligned} \arg\min_{\boldsymbol{x},\boldsymbol{u},\boldsymbol{v}} & \frac{1}{2}\left\|\frac{\boldsymbol{z} - kIe^{-\boldsymbol{u}}}{\sqrt{k^2Ie^{-\boldsymbol{u}} + \boldsymbol{\sigma}^2}}\right\|_2^2 \\ & + \frac{1}{2}\langle \log(k^2Ie^{-\boldsymbol{u}} + \boldsymbol{\sigma}^2), \boldsymbol{1}\rangle + \lambda\delta^2(\sqrt{(\frac{\boldsymbol{v}}{\delta})^2 + 1} - 1) \\ \text{s.t.} \quad & \boldsymbol{u} = \boldsymbol{A}\boldsymbol{x}, \boldsymbol{v} = \boldsymbol{C}\boldsymbol{x}. \end{aligned} \tag{9}$$

In this paper, $e^{(\cdot)}, \log(\cdot), \sqrt{\cdot}$ and division are all pointwise operation. We rewrite (9) as

$$\begin{aligned} & \arg\min_{\boldsymbol{x},\boldsymbol{s}} f(\boldsymbol{s}) \\ & \text{s.t.} \quad \boldsymbol{s} := \boldsymbol{P}\boldsymbol{x} \end{aligned} \tag{10}$$

where $\boldsymbol{s} \triangleq (\boldsymbol{u}, \boldsymbol{v})^T$, $\boldsymbol{P} \triangleq (\boldsymbol{A}, \boldsymbol{C})^T$.

2) Alternating Direction Method of Multipliers: To solve the optimzation problem in (10), we use Alternating Direction Method of Multipliers (ADMM). Given $\boldsymbol{x}^{(0)}, \boldsymbol{s}^{(0)}$ and $\boldsymbol{b}^{(0)}$ ADMM updates the sequence $(\boldsymbol{x}^{(j)}, \boldsymbol{s}^{(j)}, \boldsymbol{b}^{(j)})$ by

$$\boldsymbol{x}^{(j+1)} = \arg\min_{\boldsymbol{x}} \langle \boldsymbol{b}^{(j)}, \boldsymbol{P}\boldsymbol{x} - \boldsymbol{s}^{j} \rangle + \frac{\mu}{2} \|\boldsymbol{P}\boldsymbol{x} - \boldsymbol{s}^{j}\|_2^2, \quad (11)$$

$$\boldsymbol{s}^{(j+1)} = \arg\min_{\boldsymbol{s}} f(\boldsymbol{s}) + \langle \boldsymbol{b}^{(j)}, \boldsymbol{P}\boldsymbol{x}^{(j+1)} - \boldsymbol{s} \rangle + \frac{\mu}{2} \|\boldsymbol{P}\boldsymbol{x}^{(j+1)} - \boldsymbol{s}\|_2^2, \quad (12)$$

$$\boldsymbol{b}^{(j+1)} = \boldsymbol{b}^{(j)} + \mu(\boldsymbol{P}\boldsymbol{x}^{(j+1)} - \boldsymbol{s}^{(j+1)}). \quad (13)$$

where $\mu > 0$ is the penalty parameter and $\boldsymbol{b} = (\boldsymbol{b}_1, \boldsymbol{b}_2)^T$, $\boldsymbol{b}_1 \in \mathbb{R}^{N_d}, \boldsymbol{b}_2 \in \mathbb{R}^{N_r}$ have the same size as $\boldsymbol{A}\boldsymbol{x}, \boldsymbol{C}\boldsymbol{x}$ respectively. Note that we can also select a vector $\boldsymbol{\mu} = (\mu_1, \mu_2)$ for the two quadratic penalty constraints.

3) Algorithm: Firstly, we solve (11) to obtain $\boldsymbol{x}^{(j+1)}$. Since (11) is quadratic and differentiable on $\boldsymbol{x}$, so we solve it analytically, i.e.,

$$\boldsymbol{x}^{(j+1)*} = \boldsymbol{G}^{-1}\left[\mu_1 \boldsymbol{A}^\top(\boldsymbol{u}^{(j)} - \boldsymbol{b}_1^{(j)}) + \mu_2 \boldsymbol{C}^\top(\boldsymbol{v}^{(j)} - \boldsymbol{b}_2^{(j)})\right] \quad (14)$$

where $\boldsymbol{x}^{(j+1)*}$ represents the exact solution and $\boldsymbol{G} = \mu_1 \boldsymbol{A}^\top \boldsymbol{A} + \mu_2 \boldsymbol{C}^\top \boldsymbol{C}$ is nonsingular because because $A^\top A$ and $C^\top C$ have disjoint null space [14]. Although (14) is an exact analytical solution, it is impractical to store and invert it exactly due to its huge size for CT reconstruction. This step (14) can be solved by CG method and we obtain an approximate update $\boldsymbol{x}^{(j+1)}$.

Due to the structure of $f(\boldsymbol{s})$ and $\boldsymbol{P}$, (12) can be solved separately for $\boldsymbol{u}, \boldsymbol{v}$ as follows:

$$\boldsymbol{u}^{(j+1)} = \arg\min_{\boldsymbol{u}} \frac{1}{2} \| \frac{\boldsymbol{z} - kIe^{-\boldsymbol{u}}}{\sqrt{k^2 Ie^{-\boldsymbol{u}} + \boldsymbol{\sigma}^2}} \|_2^2 + \frac{1}{2}\langle \log(k^2 Ie^{-\boldsymbol{u}} + \boldsymbol{\sigma}^2), \boldsymbol{1} \rangle + \langle \boldsymbol{b}_1^{(j)}, A\boldsymbol{x}^{(j+1)} - \boldsymbol{u} \rangle + \frac{\mu_1}{2} \|A\boldsymbol{x}^{(j+1)} - \boldsymbol{u}\|_2^2, \quad (15)$$

$$\boldsymbol{v}^{(j+1)} = \arg\min_{\boldsymbol{v}} \lambda\delta^2 (\sqrt{(\frac{\boldsymbol{v}}{\delta})^2 + 1} - 1) + \langle \boldsymbol{b}_2^{(j)}, \boldsymbol{C}\boldsymbol{x}^{(j+1)} - \boldsymbol{v} \rangle + \frac{\mu_2}{2} \|\boldsymbol{C}\boldsymbol{x}^{(j+1)} - \boldsymbol{v}\|_2^2. \quad (16)$$

We can see that $\boldsymbol{u}, \boldsymbol{v}$ can be solved separately and in parallel. Subproblem (15) is smooth, differentiable nonconvex and separable. We apply BFGS to solve the subproblem (15).

Minimization with respect to $\boldsymbol{v}$ in (16) is the proximal operator of the edge-preserving hyperbola function, and we can update v_j separately. The dual variables is updated straightforwardly as (13). Figure 1 summarizes the optimization algorithm of the proposed MPG method.

1. Select $\boldsymbol{x}^{(0)}$, λ, μ and set $j = 0$
2. Set $\boldsymbol{u}^{(0)} = \boldsymbol{A}\boldsymbol{x}^{(0)}$,$\boldsymbol{v}^{(0)} = \boldsymbol{C}\boldsymbol{x}^{(0)}$ and $\boldsymbol{b}^{(0)} = (\boldsymbol{b}_1^{(0)}, \boldsymbol{b}_2^{(0)}) = 0$

Repeat:

3. Obtain $\boldsymbol{x}^{(j+1)}$ by applying CG iterations to (14)
4. Computer $\boldsymbol{u}^{(j+1)}$ by applying BFGS iterations to (15)
5. Computer $\boldsymbol{v}^{(j+1)}$ by (16)
6. Compute $\boldsymbol{b}_1^{(j+1)}$ and $\boldsymbol{b}_2^{(j+1)}$ using (13)
7. Set $j = j + 1$

Until stop criterion is met.

Fig. 1: ADMM for the proposed MPG reconstruction method

III. Results

In this section, we present numerical results for 3-D cone-beam CT reconstruction using simulated Shepp-logan phantom data. We used filtered back projection (FBP) reconstruction that initialized the proposed MPG method and penalized weighted-least square (PWLS) reconstruction with the edge-preserving hyperbola function [15], and compared performance of these three methods.

We used a $512 \times 512 \times 64$ Shepp-logan phantom and numerically generated a $888 \times 64 \times 984$ noisy sinogram with GE LightSpeed cone-beam geometry corresponding to a monoenergetic source with 10^4 incident photons per ray and no background events, i.e, $r_i = 0, i = 1, \cdots \mathbb{N}_d$. We chose 1000 for the scalar factor k [16] modeling the conversion gain from X-ray photons to electrons in (2) and 330^2 for σ^2 [17], the variance of electronic noise. Some elements of the measurements $\boldsymbol{z}$ are negative due to the small value of $I_i = 10^4$ simulating ULDCT imaging. The proposed MPG method can directly use these data in the reconstruction without any pre-processing. FBP and PWLS are post-log methods that need to take logarithm of the measurements $\boldsymbol{z}$. To obtain line integrals $\boldsymbol{A}\boldsymbol{x}$ for FBP and PWLS reconstruction [18], we substituted the non-positive measurement elements with a small positive value, i.e.,

$$\log(\frac{kI_i}{\max(z_i - y_N, \varepsilon)}). \quad (17)$$

For the weight in PWLS [18], we also set non-positive measurement elements with a small positive value, i.e.,

$$w_i = \frac{\max(z_i - y_N, \varepsilon)^2}{\max(z_i - y_N, \varepsilon) + \sigma^2}. \quad (18)$$

Here, in (17) and (18), ε is a small positive value and $y_N \sim N(0, \sigma^2)$. The matrix $\boldsymbol{C}$ in (8) was set as the gradient operator along three directions for 3D CT images, the regularization parameter λ was set as 2×10^5 to balance the noise and resolution, and the iteration number was 100 to reconstruct the image. Figure 2 shows the true image and the reconstructions by FBP, PWLS and the proposed MPG method. PWLS method decreases noise and removes artifacts from the FBP initialization as expected, while the proposed MPG method further improves image quality.

IV. Discussion and Conclusion

We proposed a novel SIR method, called MPG (mixed Poisson-Gaussian) for ULDCT imaging. MPG method models the noisy measurements using mixed Poisson-Gaussian distribution which accounts for the electronic noise that dominates when the X-ray dose is at an ultra-low level. We used the

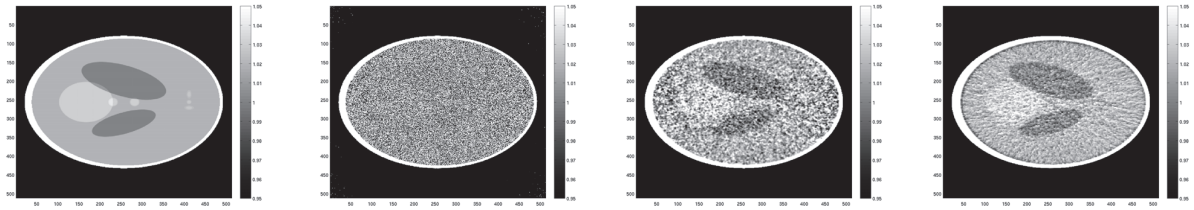

RMS	32.6%	22.3%	15.2%
(a) Ground truth	(b) FBP	(c) PWLS	(d) MPG

Fig. 2: Shepp-Logan phantom reconstructed by FBP, PWLS and the proposed MPG method. (a) Noisefree Shepp-Logan phantom, (b) FBP, (c) PWLS, and (d) Proposed MPG. Images in (b)-(d) have been displayed using the same color scale [as that of (a)]. The second row is the normalized root mean square (RMS) error of the images reconstructed by different method.

reweighted least square method to develop a tractable likelihood function that can be incorporated into SIR reconstruction framework. The proposed MPG method can accommodate edge-preserving hyperbola regularization that preserves edges and can be useful for under-sampled data by reducing the number of views for further dose reduction. We minimize the MPG cost function using ADMM which divides the original optimization problem into several sub-problems that are easier to solve. The proposed MPG method is able to directly use negative and zero values in the raw data without any pre-processing. Preliminary reconstruction results on 3D simulated data set indicate that the proposed MPG method outperforms the conventional FBP and statistical PWLS method.

In future work, we will investigate efficient methods for optimizing subproblem (15) and (16). These two subproblems are a set of 1-D Separable problems that can be solved efficiently by parallel methods. In CT, a nonnegativity constraint is often imposed to model the positivity of the attenuation coefficient that is being reconstructed. We can easily incorporate the nonnegativity constraint in the model (6).

ACKNOWLEDGMENT

This work was finished during a stay of Q. Ding at Germany funded by the China Scholarship Council, whose support is acknowledged. Q. Ding and X. Zhang were partially supported by NSFC (No. 91330102 and GZ1025) and 973 program (No. 2015CB856004). Y. Long was supported in part by SJTU-UM Collaborative Research Program, NSFC (61501292), Shanghai Pujiang Talent Program (15PJ1403900), Returned Overseas Chinese Scholars Program, and SJTU Medicine-Engineering Cross Discipline Program (YG2015QN05).

REFERENCES

[1] David J Brenner and Eric J Hall, "Computed tomography-an increasing source of radiation exposure," *New England Journal of Medicine*, vol. 357, no. 22, pp. 2277–2284, 2007.

[2] Jean-Baptiste Thibault, Ken D Sauer, Charles A Bouman, and Jiang Hsieh, "A three-dimensional statistical approach to improved image quality for multislice helical CT," *Medical physics*, vol. 34, no. 11, pp. 4526–4544, 2007.

[3] Y Long, L Cheng, X Rui, B De Man, AM Alessio, E Asma, and PE Kinahan, "Analysis of ultra-low dose CT acquisition protocol and reconstruction algorithm combinations for PET attenuation correction," in *Proc. Intl. Mtg. on Fully 3D Image Recon. in Rad. and Nuc. Med*, 2013, pp. 400–3.

[4] Bruce R Whiting, Parinaz Massoumzadeh, Orville A Earl, Joseph A OSullivan, Donald L Snyder, and Jeffrey F Williamson, "Properties of preprocessed sinogram data in X-ray computed tomography," *Medical physics*, vol. 33, no. 9, pp. 3290–3303, 2006.

[5] Johan Nuyts, Bruno De Man, Jeffrey A Fessler, Wojciech Zbijewski, and Freek J Beekman, "Modelling the physics in the iterative reconstruction for transmission computed tomography," *Physics in medicine and biology*, vol. 58, no. 12, pp. R63, 2013.

[6] Jing Wang, Tianfang Li, Hongbing Lu, and Zhengrong Liang, "Penalized weighted least-squares approach to sinogram noise reduction and image reconstruction for low-dose X-ray computed tomography," *Medical Imaging, IEEE Transactions on*, vol. 25, no. 10, pp. 1272–1283, 2006.

[7] Idris A Elbakri and Jeffrey A Fessler, "Efficient and accurate likelihood for iterative image reconstruction in X-ray computed tomography," in *Medical Imaging 2003*. International Society for Optics and Photonics, 2003, pp. 1839–1850.

[8] Patrick J La Rivière, "Monotonic iterative reconstruction algorithms for targeted reconstruction in emission and transmission computed tomography," in *Nuclear Science Symposium Conference Record, 2006. IEEE*. IEEE, 2006, vol. 5, pp. 2924–2928.

[9] Alessandro Foi, Mejdi Trimeche, Vladimir Katkovnik, and Karen Egiazarian, "Practical Poissonian-Gaussian noise modeling and fitting for single-image raw-data," *Image Processing, IEEE Transactions on*, vol. 17, no. 10, pp. 1737–1754, 2008.

[10] Jia Li, Zuowei Shen, Rujie Yin, and Xiaoqun Zhang, "A reweighted L2 method for image restoration with Poisson and mixed Poisson-Gaussian noise," *Inverse Problems and Imaging*, vol. 9, no. 3, 2015.

[11] Tom Goldstein and Stanley Osher, "The split bregman method for L1-regularized problems," *SIAM Journal on Imaging Sciences*, vol. 2, no. 2, pp. 323–343, 2009.

[12] Peter M Joseph and Robin D Spital, "A method for correcting bone induced artifacts in computed tomography scanners.," *Journal of computer assisted tomography*, vol. 2, no. 1, pp. 100–108, 1978.

[13] Idris A Elbakri and Jeffrey A Fessler, "Statistical image reconstruction for polyenergetic X-ray computed tomography," *Medical Imaging, IEEE Transactions on*, vol. 21, no. 2, pp. 89–99, 2002.

[14] Sathish Ramani and Jeffrey A Fessler, "A splitting-based iterative algorithm for accelerated statistical X-ray CT reconstruction," *Medical Imaging, IEEE Transactions on*, vol. 31, no. 3, pp. 677–688, 2012.

[15] Jeffrey A Fessler, "Statistical image reconstruction methods for transmission tomography," *Handbook of medical imaging*, vol. 2, pp. 1–70, 2000.

[16] C.C. Shaw, *Cone Beam Computed Tomography*, Imaging in Medical Diagnosis and Therapy. CRC Press, 2014.

[17] Jingyan Xu and Benjamin MW Tsui, "Electronic noise modeling in statistical iterative reconstruction," *Image Processing, IEEE Transactions on*, vol. 18, no. 6, pp. 1228–1238, 2009.

[18] Adam M. Alessio Paul E. Kinahan Lin Fu, Soo Mee Kim and Bruno De Man, "Comparison between Pre-log and Post-log statistical models in Low-Dose CT iterative reconstruction," *Nuclear Science Symposium and Medical Imaging Conference (NSS/MIC)*, pp. 1–10, 2015.